LBNL-60513
June 2006

Development of a 2D Vlasov Solver for Longitudinal Beam Dynamics in Single-Pass Systems*

M. Venturini, R. Warnock,† and A. Zholents
Lawrence Berkeley National Laboratory,
Berkeley, CA, 94720

Abstract

Direct numerical methods for solving the Vlasov equation offer some advantages over macroparticle simulations, as they do not suffer from the numerical noise inherent in using a number of macroparticles smaller than the bunch population. Unfortunately these methods are more time-consuming and generally considered impractical in a full 6D phase space. However, in a lower-dimension phase space they may become attractive if the beam dynamics is sensitive to the presence of small charge-density fluctuations and a high resolution is needed. In this paper we present a 2D Vlasov solver for studying the longitudinal beam dynamics in single-pass systems of interest for X-FEL's, where characterization of the microbunching instability is of particular relevance. The solver includes a model to account for the smearing effect of a finite horizontal emittance on microbuncing. We explore the effect of space charge and coherent synchrotron radiation (CSR). The numerical solutions are compared with results from linear theory and good agreement is found in the regime where linear theory applies.

*Work supported by Department of Energy Contract Nos. DE-AC02-05CH11231 and DE-AC02-76SF00515.

†Also at Stanford Linear Accelerator Center, PO Box 20450, Stanford, CA 94309.

1 Introduction

Lasing in an X-Ray Free Electron Laser (X-FEL) critically depends on electron-beam quality. Unfortunately, a number of effects can spoil transverse emittance and energy spread as the electron beams are accelerated and compressed before entering the undulator. Of particular concern is the development of microbunching instabilities [1, 2, 3, 4] stemming from the unavoidable irregularities present in the charge density at injection. Because of self-fields from radiation or space-charge, these irregularities may create energy fluctuations, which in turn can feed further lumping in the charge density as the beam travels through a dispersive region. Minimizing the development of such instabilities is a significant part in the effort of designing an X-FEL.

Modelling of beam dynamics is currently carried out using a combination of macroparticle simulations and semi-analytical study of the solutions of the linearized Vlasov equation. While these are essential tools for an X-FEL designer they present some well-known limitations. Macroparticle simulations are vulnerable to the numerical noise resulting from using a limited number of macroparticles. Numerical noise can be somewhat controlled by a judicious choice of suitable filters [4] but it remains difficult to separate from the genuinely physical fluctuations that one intends to study. On the other hand, the linearized Vlasov equation fails to capture nonlinear saturation, which can be important.

A possible third approach, immune to these limitations, would be to solve numerically the complete Vlasov equation. While direct numerical methods for the Vlasov equations have enjoyed a certain degree of popularity in plasma physics after the seminal paper by Cheng and Knorr [5], they have yet to find widespread application in beam physics [6, 7, 8, 9, 10, 11, 12]. To some extent this is a consequence of the larger computational cost: indeed, at present an application to a 6D phase space would be prohibitive whereas application to 4D appears feasible only using parallel computing [13]. The use of these methods in 2D phase space has been very rewarding, however, which encourages further efforts to develop solution technology both in more demanding 2D contexts and in higher dimensions.

In this paper we present progress toward the realization of a Vlasov solver for applications in single-pass systems of interest for X-FEL's, and more specifically discuss a scheme for a Vlasov solver in the 2D longitudinal phase space.

While a more complete treatment of the relevant physics would require at least a 4D phase space to fully describe the coupling between horizonal and longitudinal motion, a 2D solver is already physically significant for some applications. Moreover, it is shown in this paper that the smoothing effect of a finite transverse emittance, which is often crucial to include, could be modelled to some extent without the need to follow the transverse dynamics. In any event, a 2D solver shares some of the algorithmic challenges with solvers in higher dimensions, making it the first necessary step toward any more ambitious goal.

Modelling of a beam for FEL applications has to face the presence of a close correlation between longitudinal position and energy, which is deliberately added to achieve compression in magnetic chicanes. This correlation makes the simple method [8, 9, 10] of gridding the phase space on a static rectangular mesh ill suited. Two distinct strategies can be devised involving either grid adaptation or a suitable coordinate transformation. A combination of

the two might also be profitable. With regard to the first, recent work by Sonnendrücker and coworkers [14] using multiscale resolution and moving grids is promising, while grid-free methods proposed in [15] may be worthy of further exploration. Concerning the second strategy a change of variables to the "interaction picture" was proposed in [12]. In the present paper we explore a method that involves a transformation to new dynamical variables that is different from the one suggested in [12], and uses cell-size adaptation in a cartesian grid that avoids the complications of local mesh refinement. The idea for the coordinate transformation is simply to subtract the energy-position correlation from the energy coordinate, whereas the grid adaptation follows the natural beam compression occurring as the beam travels through the magnetic chicane.

In Sec. 2 we derive the 2D Vlasov equation for beams with vanishing transverse emittance and in Sec. 3 give a detailed description of the integration method in a bunch compressor. We follow with a schematic summary of the algorithm (Sec. 4) and after mentioning the relevant equations for handling motion in the RF cavities (Sec. 5), we investigate the sensitivity of the method to the numerics, making contact with linear theory (Sec. 6). Finally, in Sec. 7 we present a model for including the effect of a finite horizontal emittance on the development of microbunching and, again, make comparison with linear theory. Throughout the paper the numerical examples are based on the lattice for the fermi@elettra X-FEL under design at Elettra [16].

2 The 2D Vlasov Equation for Bunch Compressors

Neglecting coupling with vertical motion (a generally good approximation) we describe the horizontal and longitudinal dynamics in a bunch compressor in the ultrarelativistic regime in terms of the Hamiltonian

$$H = \frac{1}{2}\left(p_x^2 + k_x(s)x^2\right) - \frac{x}{R(s)}\delta - \frac{1}{p_0}\int_{-\infty}^{z} F(z')dz' \tag{1}$$

with the last term on the RHS accounting for collective effects. In the above equation $k_x(s)$ is the focusing function, $R(s)$ the local radius of curvature of the design orbit, $\delta = (p-p_0)/p_0$ an electron relative energy deviation from the design energy p_0. [‡].

The collective longitudinal force $F(z)$ acting on an electron at z within a bunch depends on the component of the electric field parallel to the particle trajectory at that point. Here, z is the longitudinal distance of the electron from a synchronous particle following the design orbit. In our convention $z > 0$ indicates a particle closer to the bunch head. If we denote with $w(z - z')$ the longitudinal component of the electric field at z generated by a *positive* unit charge placed at z', then the longitudinal electric field $E_s(z)$ experienced by an electron at z is

$$E_s(z) = -eN\int_{-\infty}^{\infty} dz' w(z - z')\rho(z'), \tag{2}$$

where N is the number of electrons in the bunch, $-e$ their charge, and $\rho(z)$ the longitudinal beam density normalized to unity $\int_{-\infty}^{\infty} dz\rho(z) = 1$. Adopting the convention that E_s is

[‡]Throughout this paper p will always denote an energy, not a momentum

positive if pointing in the direction of increasing s, the energy change per unit length induced on a particle by the electric field is

$$\frac{d\delta}{ds} = -\frac{eE_s(z)}{p_0} = \frac{e^2N}{p_0}\int_{-\infty}^{\infty} dz' w(z-z')\rho(z'), \tag{3}$$

yielding

$$F(z) = e^2N\int_{-\infty}^{\infty} dz' w(z-z')\rho(z'). \tag{4}$$

To avoid any confusion, notice that $w(z-z')$, here defined to denote an electric *field* per unit charge, is sometimes used to represent an electric *potential* per unit charge [17].

Alternatively, we can choose to work in the frequency domain using instead the impedance per unit length $\hat{Z}(k)$[§] which is defined by:

$$\tilde{E}_s(k) = -\hat{Z}(k)\tilde{I}(k), \tag{5}$$

where $\tilde{E}_s(k)$ and $\tilde{I}(k)$ are the Fourier transform of the longitudinal field $E_s(z)$ and current $I(z)$, with $\tilde{I}(k) = -eN\beta c\tilde{\rho}(k)$:

$$\tilde{E}_s(k) = \frac{1}{2\pi}\int_{-\infty}^{\infty} dz e^{-ikz}E_s(z), \tag{6}$$

$$\tilde{\rho}(k) = \frac{1}{2\pi}\int dz e^{-ikz}\rho(z). \tag{7}$$

By the inverse Fourier transformation of (4) we then have

$$F(z) = -eE_s(z) = -e^2N\beta c\int_{-\infty}^{\infty} dk\hat{Z}(k)\tilde{\rho}(k)e^{ikz}. \tag{8}$$

It follows from (4), (7), and (8) that

$$w(z) = -\frac{c\beta}{2\pi}\int_{-\infty}^{\infty} dk\hat{Z}(k)e^{ikz}. \tag{9}$$

The minus sign on the RHS of the above equation follows from our convention that a positive w correspond to energy gain for a particle. Incidentally, notice that there may be models for the impedance in which the integral (9) does not exist where (8) may still be well defined thanks to the cut-off provided by $\tilde{\rho}(k)$.

The Vlasov equation for the phase space density $f(x, p_x, z, \delta; s)$ with Hamiltonian H can be readily written

$$\frac{\partial f}{\partial s} + p_x\frac{\partial f}{\partial x} + \left(\frac{\delta}{R(s)} - xk_x(s)\right)\frac{\partial f}{\partial p_x} - \frac{x}{R(s)}\frac{\partial f}{\partial z} + \frac{F(z)}{p_0}\frac{\partial f}{\partial \delta} = 0. \tag{10}$$

In this section we are interested in examining beams with vanishing transverse emittance. In order to derive the Vlasov equation governing such beams it is useful to introduce a new

[§]We use a ˆ to remind ourselves that $\hat{Z}$ is an impedance per unit length.

set of coordinates describing the purely betatron part of the horizontal motion [18]:

$$\begin{aligned} x_\beta &= x - \delta D, && (11)\\ p_{x\beta} &= p_x - \delta D', && (12)\\ z_\beta &= z + xD' - p_x D, && (13)\\ \delta_\beta &= \delta, && (14) \end{aligned}$$

where D is the dispersion function which satisfies $D'' + k_x D = 1/R$. The transformation to the new coordinates has generating function of the second kind

$$F_2 = p_{x\beta}(x - \delta_\beta D) + x\delta_\beta D' + \left(z - \delta_\beta \frac{DD'}{2}\right)\delta_\beta, \tag{15}$$

with $x_\beta = \partial F_2/\partial p_{x\beta}$, $p_x = \partial F_2/\partial x$, etc. This transformation yields the new Hamiltonian

$$H_\beta = H + \frac{\partial F_2}{\partial s} = \frac{1}{2}\left(p_{x\beta}^2 + k_x(s)x_\beta^2\right) - \frac{D}{2R}\delta_\beta^2 - \frac{1}{p_0}\int_{-\infty}^{z} F(z')dz'\Big|_{z=z_\beta - x_\beta D' + p_{x\beta}D}. \tag{16}$$

Having set $\zeta = z_\beta - x_\beta D' + p_{x\beta}D$, the resulting Vlasov equation is then

$$\begin{aligned} &\frac{\partial f}{\partial s} + \left[p_{x\beta} - \frac{F(\zeta)}{p_0}D\right]\frac{\partial f}{\partial x_\beta} - \left[k_x x_\beta + \frac{F(\zeta)}{p_0}D'\right]\frac{\partial f}{\partial p_{x\beta}} + \\ &-\delta_\beta \frac{D}{R}\frac{\partial f}{\partial z_\beta} + \frac{F(\zeta)}{p_0}\frac{\partial f}{\partial \delta_\beta} = 0, \end{aligned} \tag{17}$$

where we now regard f as a function of the new variables.

The distribution of a beam with vanishing transverse emittance can be written as

$$f = \hat{\delta}(x_\beta)\hat{\delta}(p_{x\beta})f_z(z_\beta, \delta_\beta), \tag{18}$$

where $\hat{\delta}$ is the Dirac delta function. In the presence of collective effects a density function of the form (18) is not an exact solution of (17). In other words, a beam with initial vanishing horizontal emittance will see its emittance grow as a consequence of collective forces. We assume that such an emittance growth will be sufficiently small that (18) remains close to the actual solution. If this is the case, we can obtain a reduced 2D Vlasov equation for the longitudinal motion by inserting (18) into (17) and integrating over the transverse variables x_β, and $p_{x\beta}$:

$$\frac{\partial f_z}{\partial s} - \delta_\beta \frac{D}{R}\frac{\partial f_z}{\partial z_\beta} + \frac{F(z_\beta)}{p_0}\frac{\partial f_z}{\partial \delta_\beta} = 0. \tag{19}$$

We might say that (18) satisfies (17) in the sense of an average over transverse phase space, if (19) is satisfied.

For brevity, for the rest of this and the next section we will drop the subscript β in the notation for the coordinates and the subscript z from the longitudinal density f_z. Also, we

Table 1: Parameters for bunch compressor BC1 in the fermi@elettra linac

Parameter	BC1
Energy E (MeV)	233
Current before compression I_0 (A)	95.5
Normalized emittance $\varepsilon_{xn} = \gamma\varepsilon_x$ (μm)	1
Curvature radius in dipoles R (m)	7.38
Dipole length (m)	0.5
Length of first/last drifts (m)	2.5
Length of middle drift (m)	1.0
Compressor total length (m)	8.0
Compression factor	3.52

will find it convenient to regard p in $\delta = (p - p_0)/p_0$ as the dynamical variable instead of δ. In terms of the dynamical variables (z, p) Eq. (19) can be rewritten as

$$\frac{\partial f}{\partial s} - \frac{(p - p_0)}{p_0}\frac{D}{R}\frac{\partial f}{\partial z} + F(z)\frac{\partial f}{\partial p} = 0, \tag{20}$$

with the underlying Hamiltonian

$$H = H_{\text{ext}} + H_c, \tag{21}$$

where

$$H_{\text{ext}}(p) = -\frac{D}{2R}\frac{(p - p_0)^2}{p_0} \tag{22}$$

accounts for the external forces and

$$H_c(z) = -\int_{-\infty}^{z} F(z')dz' \tag{23}$$

for the collective effects.

We end this section by reporting the expressions for the impedances used to model space charge and coherent synchrotron radiation (CSR), the two collective effects most relevant for microbunching. We ignore collective forces due to the RF structure wake fields, which can be very significant but are generally effective on a length scale longer than the one relevant for microbunching.

For space charge we use the model [3, 19] of impedance (per unit length)

$$\hat{Z}(k) = \frac{iZ_0}{\pi\gamma r_b}\frac{1 - xK_1(x)}{x}\bigg|_{x=kr_b/\gamma}, \tag{24}$$

where $K_1(x)$ is a modified Bessel function and $Z_0 = 120\pi\ \Omega$, the vacuum impedance. This formula applies to a bunch with transversally uniform density and circular cross section of radius r_b in free space and yields the electric field on the beam axis. The applicability of this expression is for wavelengths small compared to b/γ [17] or else boundary effects from the vacuum chamber wall of radius b may become noticeable (γ is the relativistic factor).

For CSR we used the impedance model [2] for radiation in free space

$$\hat{Z}(k) = Z_0 \frac{\Gamma(2/3)}{3^{1/3} 4\pi R} [\sqrt{3} + i](kR)^{1/3}. \tag{25}$$

where Γ is the Euler function. Because we are mostly interested in the evolution of high frequency components of the bunch spectrum this is adequate for our study: shielding from the vacuum chamber [10] becomes noticeable for wavelengths longer than about $b(2b/R)^{1/2}$. For the fermi@elettra chicane parameters ($b \simeq 4$ mm and radius of curvature $R \simeq 7.4$ m) this number is about 130 μm – larger than wavelengths of interest for microbunching. An additional approximation is to neglect transient effects at dipole ends, as the impedance (25) properly applies to particles in uniform motion on a circular orbits: the criterion [1] for the validity of (25), $\lambda \leq R\phi^3/24$, where ϕ is the dipole bend angle, yields a critical wavelength $R\phi^3/24 = 100\mu$m (for $R \simeq 7.4$ m and $\phi = 70$ mrad).

The expressions above are understood to be valid for wavenumbers $k > 0$. For negative wavenumbers the correct expressions are recovered by the rule $Z(-k) = Z^*(k)$.

Profiles for the two impedance models are reported in Fig. 1. The parameters for the space charge impedance are those for the L1 section of the fermi@elettra linac. The radius of curvature to calculate the CSR impedance is close to that of the dipoles in the bunch compressors.

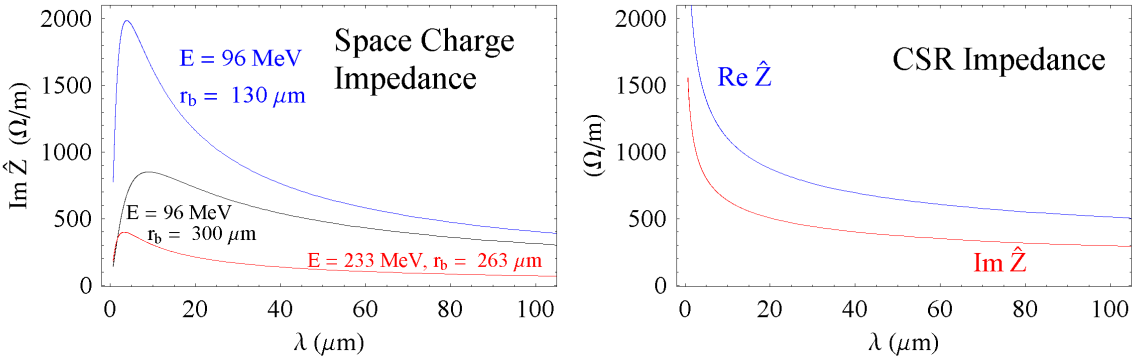

Figure 1: Space-charge and CSR impedances (per unit length). The space charge impedance is reported for various beam energy and transverse size r_b. In the plot of the CSR impedance we used $R = 7.4$ m.

3 Integrator for Bunch Compressors

In a bunch compressor the canonical equations of motion when collective effects are absent read (see Hamiltonian (22))

$$\frac{dz}{ds} = -\frac{D}{R}\frac{p - p_0}{p_0}, \tag{26}$$

$$\frac{dp}{ds} = 0. \tag{27}$$

Using the 'R'-matrix notation, the mapping $\mathcal{T} : (z, p) \to (z', p')$, with $z' = z(s')$, $z = z(s)$, $p' = p(s')$, and $p = p(s)$ representing the solution of (26) and (27) can be written as

$$z' = z + \frac{p - p_0}{p_0}[R_{56}(s') - R_{56}(s)], \tag{28}$$

$$p' = p, \tag{29}$$

where $R_{56}(s) = -\int_{s_0}^{s} d\tau D(\tau)/R(\tau)$, having assumed that at the entry $s = s_0$ of the bunch compressor $R_{56}(s_0) = 0$. Incidentally, notice that if $D = D' = 0$ at the entrance of a bend, and assuming that the transverse focusing is negligible, from $D'' = 1/R$ it follows that $D(s)$ and $R(s)$ have the same sign so that $R_{56}(s)$ is negative over the first dipole of a chicane. In the next bend the sign of the radius of curvature R changes and R_{56} grows positive. A bunch compressor is designed so that R_{56} remains positive through the last dipole of the chicane. Plots of $D(s)$ and $R_{56}(s)$ are reported in Fig 7.

While the form of the equations of motion is most simple in the variables (z, p), a numerical solution of the Vlasov equation for a chirped beam is most efficiently done using a different set of coordinates.

Consider a transformation $\mathcal{A} : (z, p) \to (\hat{z}, \hat{p})$ to a new coordinate system $(\hat{z}, \hat{p})$ defined by

$$\hat{z} = z, \tag{30}$$

$$\hat{p} = p - \alpha(z, s). \tag{31}$$

The idea is to identify the function $\alpha(z, s)$ as the beam correlation or 'chirp function' with the goal of having a coordinate system in which the support of the beam density is centered at $\hat{p} \simeq 0$. At $s = s_0$ we define

$$\alpha(z, s_0) = \int_{-\infty}^{\infty} dppf(z, p; s_0) / \int_{-\infty}^{\infty} dpf(z, p; s_0). \tag{32}$$

We can think of $(z, \alpha(z, s_0))$, a 1D curve in phase space, as the support of a beam density with vanishing uncorrelated energy spread.

Different options are possible for the evolution of function $\alpha(z, s)$ for $s > s_0$. A simple rule is to assume that each point of the 1D curve $(z, \alpha(z, s_0))$ in phase space evolves like a particle with position z and canonical momentum $\alpha(z, s_0)$ under the influence of the external forces alone. That is, given $\alpha(z, s)$ at s as a function of z, the value at z' of $\alpha(z', s')$ at a later time $s' > s$ is

$$\alpha(z', s') = \alpha(z, s), \tag{33}$$

where z in the RHS is determined for a given z' as solution of the algebraic equation

$$z' = z + \frac{\alpha(z, s) - p_0}{p_0}[R_{56}(s') - R_{56}(s)]. \tag{34}$$

The transformation (30), (31) is canonical with generating function $\hat{F}_2 = z\hat{p} + \tilde{\alpha}(z, s)$ where $\tilde{\alpha}(z, s)$ is a primitive of $\alpha(z, s)$ with respect to z (*i.e.* $\partial\tilde{\alpha}/\partial z = \alpha$). The resulting Hamiltonian

$$\hat{H} = -\frac{D}{2R}\frac{(\hat{p} + \alpha(\hat{z}, s) - p_0)^2}{p_0} + \frac{\partial\tilde{\alpha}(\hat{z}, s)}{\partial s} + \hat{H}_c(\hat{z}), \tag{35}$$

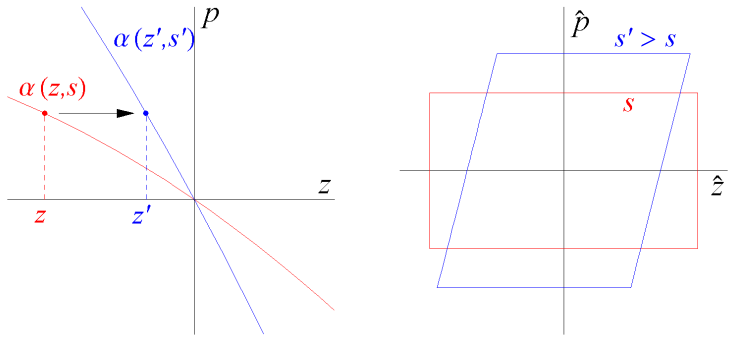

Figure 2: Schematic for the evolution of the chirp function (figure to the left) and dynamics in the $(\hat{z}, \hat{p})$ phase space for a beam with linear chirp (figure to the right).

with $\hat{H}_c(\hat{z}) = H_c(\hat{z})$, enables us to write the Vlasov equation in the new coordinates replacing (19)

$$\frac{\partial f}{\partial s} + \frac{d\hat{z}}{ds}\frac{\partial f}{\partial \hat{z}} + \frac{d\hat{p}}{ds}\frac{\partial f}{\partial \hat{p}} = 0, \tag{36}$$

where

$$\frac{d\hat{p}}{ds} = \frac{D}{R}\left(\frac{\hat{p} + \alpha(\hat{z}, s) - p_0}{p_0}\right)\frac{\partial \alpha(\hat{z}, s)}{\partial \hat{z}} - \frac{\partial \alpha(\hat{z}, s)}{\partial s} + F(\hat{z}), \tag{37}$$

$$\frac{d\hat{z}}{ds} = -\frac{D}{R}\left(\frac{\hat{p} + \alpha(\hat{z}, s) - p_0}{p_0}\right). \tag{38}$$

Undoubtedly the equations of motions are more complicated in the new coordinates. What we have gained, however, is a phase space where one can efficiently use a cartesian grid to represent the density function. This is a considerable advantage toward the goal of solving (36) numerically.

To solve (36) we apply a method first introduced in [5] (see also [8, 10]), exploiting the following basic property of volume-preserving systems. Suppose $\mathcal{M}_{s\to s'}(\boldsymbol{z}) : \boldsymbol{z} \to \boldsymbol{z}' = \mathcal{M}_{s\to s'}(\boldsymbol{z})$ is a volume preserving map[¶] describing particle trajectories from time s to time s', where $\boldsymbol{z}$ is the vector of dynamical variables; in our case $\boldsymbol{z} = (z, p)$. Then, the time evolution of a density function f in phase space is given by $f(\boldsymbol{z}', s') = f(\boldsymbol{z}, s)$, or

$$f(\boldsymbol{z}', s') = f(\mathcal{M}^{-1}_{s\to s'}(\boldsymbol{z}'), s). \tag{39}$$

In [5] and our previous work [9, 10] the Hamiltonian could be separated as $H(z, p) = T(p) + U(z)$, which suggested propagating the density function over the small increment Δs under the Hamiltonian flows alternately generated by the $T(p)$ and $U(z)$ parts of the

[¶]For Hamiltonian systems this map is often referred to as the "Hamiltonian flow".

Hamiltonian - the familiar kick-drift succession of a leap-frog integration scheme. In general, if a Hamiltonian has decomposition $H = H_1 + H_2$ the integrator one obtains by interleaving the mappings generated by H_1 and H_2 over the time interval Δs is second order in Δs (assuming that the two mappings are known exactly).[‖]

Hamiltonian (35) cannot be decomposed into two parts depending on position and canonical momentum separately. Instead, a more natural decomposition, closer in spirit to that exploited in [8], is $\hat{H} = \hat{H}_{\rm ext} + \hat{H}_c$ where we separate the dynamics generated by the external forces

$$\hat{H}_{\rm ext} = -\frac{D}{2R}\frac{(\hat{p} + \alpha(\hat{z}, s) - p_0)^2}{p_0} + \frac{\partial\tilde{\alpha}(\hat{z}, s)}{\partial s}. \tag{40}$$

from that generated by the collective forces.

At first one could fear that such decomposition would not work as the dynamics generated by $\hat{H}_{\rm ext}$ looks complicated. However, we are soon reminded that the undue complication only arises from the choice of the 'capped' coordinates, whereas the underlying dynamics $\mathcal{T}$ as expressed in the (z, p) coordinates, see Eq. (28) and (29), is in fact very simple. Indeed we can simply determine the mapping $\hat{\mathcal{T}}$ generated by $\hat{H}_{\rm ext}$ by transforming back and forth to the old variables: $\hat{\mathcal{T}} = \mathcal{A}\mathcal{T}\mathcal{A}^{-1}$, where $\mathcal{A}$ is the transformation defined in (30) and (31). A graphical representation of this similarity transformation is outlined in the commutative diagram:

$$\begin{array}{ccc} (\hat{z}, \hat{p}) & \xrightarrow{\hat{\mathcal{T}}} & (\hat{z}', \hat{p}') \\ \Big\downarrow \mathcal{A}^{-1} & & \Big\downarrow \mathcal{A}^{-1} \\ (z, p) & \xrightarrow{\mathcal{T}} & (z', p') \end{array}$$

By working out the chain of maps we find for $\hat{\mathcal{T}}$:

$$\begin{aligned} \hat{z}' &= z' = z + (p - p_0)dR_{56} \\ &= \hat{z} + [\hat{p} + \alpha(\hat{z}, s) - p_0]dR_{56}, \qquad (41) \\ \hat{p}' &= p' - \alpha\,(z', s') = p - \alpha\,(z + (p - p_0)dR_{56}, s') \\ &= \hat{p} + \alpha(\hat{z}, s) - \alpha\,(\hat{z} + [\hat{p} + \alpha(\hat{z}, s) - p_0]dR_{56}, s')\,, \qquad (42) \end{aligned}$$

where for brevity we have denoted $dR_{56} = dR_{56}(s, s') = [R_{56}(s') - R_{56}(s)]/p_0$.

The inverse $\hat{\mathcal{T}}^{-1}$ of the above map, which is of more direct interest to us, reads

$$\begin{aligned} \hat{z} &= \hat{z}' - [\hat{p}' + \alpha(\hat{z}', s) - p_0]dR_{56}, \qquad (43) \\ \hat{p} &= \hat{p}' + \alpha(\hat{z}', s') - \alpha\,(\hat{z}' + [\hat{p}' + \alpha(\hat{z}', s) - p_0]dR_{56}, s)\,. \qquad (44) \end{aligned}$$

[‖]More precisely, if we denote with $\mathcal{M}^{(1)}_{\Delta s}$ and $\mathcal{M}^{(2)}_{\Delta s}$ the two mappings the second-order integrator is $\mathcal{M}^{(1)}_{\Delta s}\mathcal{M}^{(2)}_{\Delta s/2}\mathcal{M}^{(1)}_{\Delta s}$.

To get a better grasp of this mapping consider the simple case of a beam with a linear chirp: *i.e.*

$$\alpha(z,s) = \alpha_1(s)z + p_0. \tag{45}$$

We can determine the chirp function at a later $s' > s$ by solving Eq.'s (33), (34). We find that the chirp function at s' is still a linear function of z: $\alpha(z',s') = \alpha_1(s')z' + p_0$ with

$$\alpha_1(s') = \frac{\alpha_1(s)}{1+\alpha_1(s)dR_{56}(s,s')}. \tag{46}$$

By using equations (41) and (42) we find

$$\hat{z}' = \hat{z}[1+\alpha_1(s)dR_{56}(s,s')] + \hat{p}\; dR_{56}(s,s'), \tag{47}$$

$$\hat{p}' = \frac{\hat{p}}{1+\alpha_1(s)dR_{56}(s,s')}. \tag{48}$$

We observe that unlike the canonical momentum p, the coordinate $\hat{p}$ expressing the uncorrelated energy spread, is not invariant. In particular, the $\hat{p}$-direction stretches (in a bunch compressor the number $1+\alpha_1(s)dR_{56}(s,s')$ is generally smaller than unity) while $\hat{z}$ is compressed. Moreover, as indicated in the last term in (47) the degree of compression on $\hat{z}$ depends, albeit weekly, on $\hat{p}$. A graphical illustration of the action of the linear transformation (47) and (48) is presented in the right picture of Fig. 2.

4 Algorithm

We represent the density function in the variables $(\hat{z},\hat{p})$ on a cartesian grid with a fixed number of $(2N_{\hat{z}}+1)\times(2N_{\hat{p}}+1)$ nodes but with varying cell sizes $\Delta_{\hat{z}}^k$ and $\Delta_{\hat{p}}^k$ (the index k refers to the time step). Grid adaptation follows the support of the beam density function in phase space as the beam contracts in position $\hat{z}$ and expands in the canonical momentum $\hat{p}$. Following the time-splitting method [5] we first advance the density function by Δs under the mapping $\hat{\mathcal{T}}$ for the unperturbed lattice defined in (41) and (42), and then advance the density function under the collective force kick.

Suppose that at 'time' $s = k\Delta s$ the density function $f_{ij} = f(\hat{z}_i,\hat{p}_j)$, is known on the grid nodes $\hat{z}_i,\hat{p}_j$ specified as $\hat{z}_i = i\Delta_{\hat{z}}^k$, with $i = -N_{\hat{z}}, -N_{\hat{z}}+1, ..., N_{\hat{z}}$ and $\hat{p}_j = j\Delta_{\hat{p}}^k$ with $j = -N_{\hat{p}}, -N_{\hat{p}}+1, ..., N_{\hat{p}}$. Assume that the chirp function $\alpha(\hat{z}_i,s)$ on the grid $\hat{z}_i$ is also known.

To propagate the density from previous time $s = k\Delta s$ to current time $s' = s+\Delta s = (k+1)\Delta s$ we undertake the following steps:

1. Adapt the new grid sizes according to

$$\Delta_{\hat{z}}^{k+1} = \Delta_{\hat{z}}^k/C, \tag{49}$$

$$\Delta_{\hat{p}}^{k+1} = \Delta_{\hat{p}}^k C, \tag{50}$$

where the compression factor $C = \left[1+dR_{56}(s,s')\frac{d\alpha(\hat{z},s)}{d\hat{z}}|_{\hat{z}=0}\right]^{-1}$ depends on the slope of the chirp function $\alpha(\hat{z},s)$ at $\hat{z}=0$. The slope is calculated from the coefficients of the spline interpolation of $\alpha(\hat{z}_i,s)$.

2. Advance the chirp function from s to current time s' according to (33) and (34). To do this, first we find the images of the grid points $\hat{z}_i$ under the map (34); these images in general will not fall on grid points of the grid at current time s' but can be used to create a cubic spline representation for α at s'. The chirp function is then evaluated on the grid points of the current grid at s' by spline interpolation.

3. Determine the backward images of the nodes ($\hat{z}'_i = i\Delta_{\hat{z}}^{k+1}, \hat{p}'_j = j\Delta_{\hat{p}}^{k+1}$) under the mapping $\mathcal{T}^{-1}$ defined in (43) and (44):

$$\hat{z} = \hat{z}'_i - [\hat{p}'_j + \alpha(\hat{z}'_i, s) - p_0]dR_{56}, \tag{51}$$

$$\hat{p} = \hat{p}'_j + \alpha(\hat{z}'_i, s') - \alpha\left(\hat{z}'_i + [\hat{p}'_j + \alpha(\hat{z}'_i, s) - p_0]dR_{56}, s\right). \tag{52}$$

   Notice that to evaluate this mapping we make use of the chirp function α both at present s' and previous time s. In (52) we use spline interpolation when the argument of α falls between grid points.

4. In the grid at s identify the nodes neighboring the point $(\hat{z}, \hat{p})$ calculated in (51) and (52). Use the values of the density function at time s on these nodes to determine $f(\hat{z}, \hat{p}; s)$ by interpolation. We found a local 16-point interpolation scheme using bicubic polynomials quite effective. Identify the value $f(\hat{z}'_i, \hat{p}'_j; s')$ of the density function at current time s' on the node $(\hat{z}'_i, \hat{p}'_j)$ as $f(\hat{z}'_i, \hat{p}'_j; s') = f(\hat{z}, \hat{p}; s)$.

5. Integrate the phase density $f(\hat{z}'_i, \hat{p}'_j; s')$ with respect to canonical momentum to obtain the longitudinal charge density.

6. Calculate the FT of the charge density and combine it with the impedance to determine the collective force and the corresponding kick at $\hat{z}'_i$

7. Advance the beam density function under the kick. Because the kick depends only on the position (not the canonical momentum) coordinate, only 1D interpolations are necessary to determine the density function. This interpolation is done by cubic splines.

Evaluation of the Fourier transform of the charge density in item 6. and determination of the collective force is done by FFT along the lines of Ref. [10].

For an example of numerical solution obtained using our integration method see Fig. 3. The picture shows the phase space for a beam at the entrance and exit of BC1, the first bunch compressor of the fermi@elettra linac. The phase space in the transformed ('capped') coordinates (two pictures at the bottom) is contrasted to the phase space in the untransformed coordinates (top pictures). The only collective effect present here was CSR.

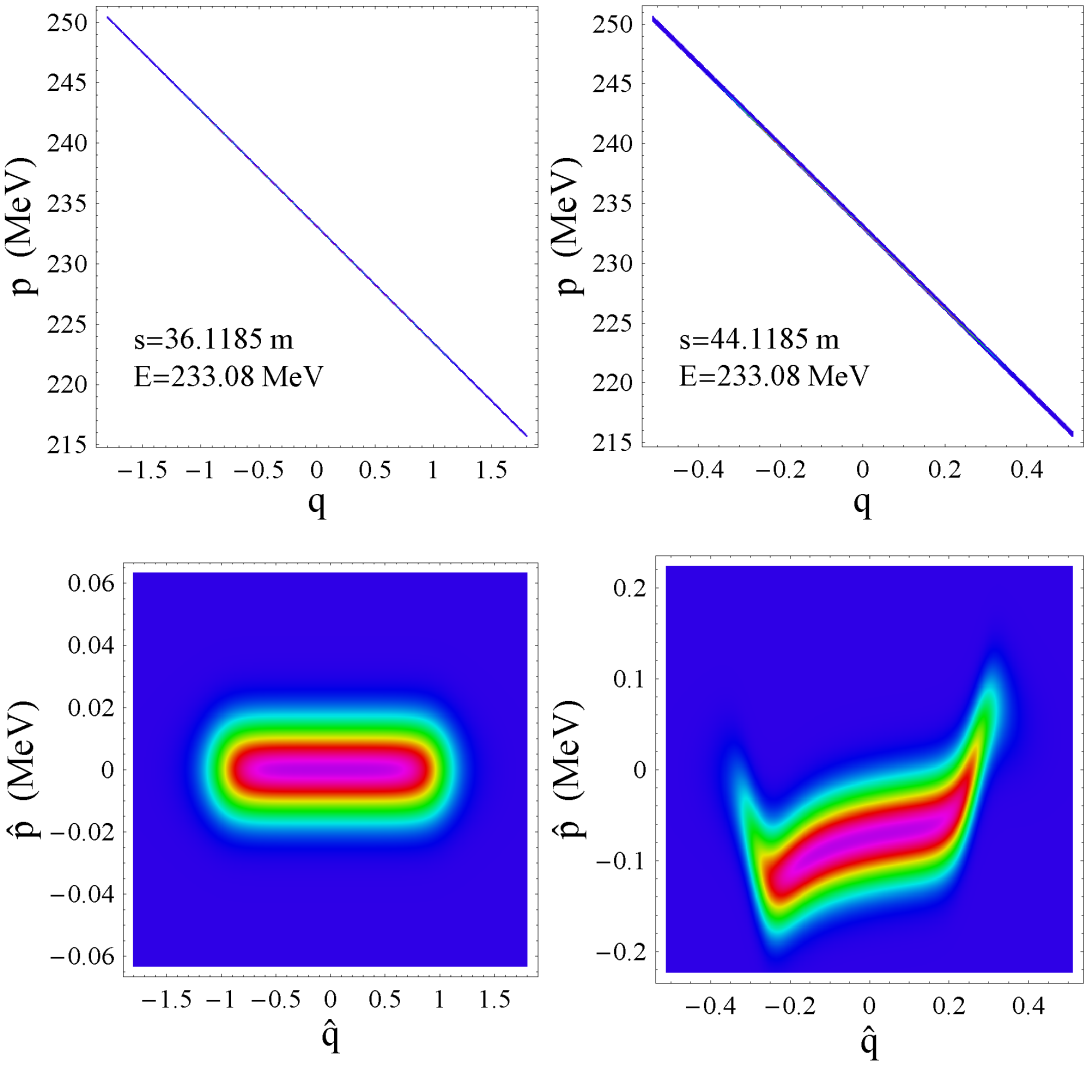

Figure 3: Beam density function in phase space at the entrance (left pictures) and exit (right pictures) of a bunch compressor. At entrance the beam has linear chirp, a smooth flat-top charge density, and gaussian uncorrelated energy spread. The phase space in the (q, p) coordinates (top pictures) is contrasted to that in the $(\hat{q}, \hat{p})$ coordinates (bottom pictures) in which the beam energy-position correlation is subtracted; $q = z/l_b$ is the scaled longitudinal coordinate with $l_b = 1.5$ mm, and $q = \hat{q}$. The beam energy is E=233 MeV. The head of the bunch is at $q > 0$.

5 Longitudinal Motion in RF Structures

In non-dispersive regions of the lattice particles in an ultrarelativistic beam can be assumed to be 'frozen' in space with respect to each other whereas their energy changes as a result of the RF fields and collective effects. As a consequence, propagation of the beam density in phase space is much simpler than in a bunch compressor.

In the absence of collective effects the equations of motion are nontrivial only within an RF cavity

$$\frac{dz}{ds} = 0, \tag{53}$$

$$\frac{dp}{ds} = \frac{\Delta E_{\rm cav}}{L_{\rm cav}} \sin(-\omega_{\rm rf} z/c + \phi_s), \tag{54}$$

where $E_{\rm cav}$ is the energy gain by a synchronous particle through a cavity of length $L_{\rm cav}$. By demanding that in an RF structure the chirp function evolves according to

$$\alpha(z', s') = \alpha(z, s) + \frac{s' - s}{L_{\rm cav}} \sin(-\omega_{\rm rf} z/c + \phi_s) \tag{55}$$

one can immediately realize that the dynamics in the 'capped' coordinates is the identity, $\hat{z}' = \hat{z}, \hat{p}' = \hat{p}$.

As in bunch compressors, collective effects are modelled using kicks in energy while propagation of the beam density in phase space is done using 1D interpolations.

6 Numerical Checks and Contact with Linear Theory

To gain confidence in the coding of the algorithm we ran a number of checks and made comparison with linear theory.

The calculations discussed here were done for using the parameters for the fermi@elettra BC1 chicane (see Table 1 in Sec. 3). As initial bunch density we used a model of flattop beam with smooth edges in z with gaussian energy spread and initial linear chirp $\alpha(z) = \alpha_1 z + p_0$: $f(z,p) = f_{\rm flt}(z, p - p_0 - \alpha_1 z)$, where $f_{\rm flt}(z,p) = \rho_{\rm flt}(z) \exp(-p^2/2\sigma_p^2)/\sqrt{2\pi}\sigma_p$ and

$$\rho_{\rm flt}(z) = \frac{1}{4 l_b} \left[\tanh\left(\frac{z + l_b}{f_r} \right) - \tanh\left(\frac{z - l_b}{f_r} \right) \right]. \tag{56}$$

In the above equation $2l_b$ is the bunch length, f_r is a parameter controlling the roll-off of the density profile at the ends. For the calculations of this section we set the beam uncorrelated energy spread to $\sigma_p = 10$ KeV (at energy $E = 233$ MeV).

One test we made was to compare the numerical to the exact solutions of the Vlasov equation through the BC1 chicane in the zero-current limit. In that limit the exact solution is determined by (39) with the linear map $\mathcal{M}^{-1}_{s \to s'}$ given by the inverse of (28) and (29). In Fig. 4 we report the maximum relative error of the numerical solution as a function of the number of grid points in the position coordinate. We compare two different 2D interpolation

schemes, one using 16 and the other 4 neighboring points (see item 4. in Sec. 4). The initial 4D beam density was perturbed by adding a small sinusoidal modulation with wavelength of the modulation about twenty times smaller that the bunch length. The $\hat{z}-$grid was about twice as as long as the bunch length while the $\hat{p}$-grid extended over 18 times the sigma of the uncorrelated energy spread σ_p. The number of grid points in $\hat{p}$ was kept fixed at $N_{\hat{p}} = 64$. A second curve, obtained using the 16-point interpolation scheme and with $N_{\hat{p}} = 128$, is also plotted in the same figure but is undistinguishable from the $N_{\hat{p}} = 64$ curve. In spite of a considerably better accuracy the 16-point interpolation runs were not appreciably longer than those using the 4-point interpolation scheme. In the rest of our calculations discussed in this paper we used exclusively the former.

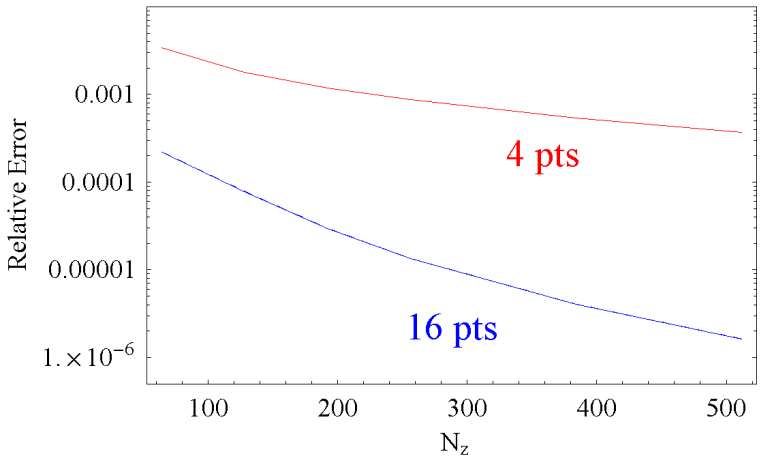

Figure 4: Scaling of the relative error of the numerical solution of the Vlasov equation for vanishing current *vs.* the number $N_{\hat{z}}$ of grid points in the position coordinate. The number of grid points in the canonical momentum was $N_{\hat{p}} = 64$. The 16- and 4-point interpolation methods are compared.

Further tests of the coding were made by looking for comparison with linear theory. A linear theory for the gain function in a bunch compressor in the presence of CSR was developed by S. Heifets *et al.* [2]. The gain curve describes the increment in amplitude of a sinusoidal perturbation of the beam charge density. The linear theory yields an integral equation for the gain function, which in [2] is solved numerically. Later Huang and Kim [3] worked out an approximate solution to this integral equation expressed as a perturbation series with the current as a small parameter, and gave explicit expressions for the first three terms of this perturbative series.

The zeroth order term of the series represents the effect of mixing in phase space caused by a finite uncorrelated energy spread in the absence of any collective effect. For coasting beams with gaussian energy spread, this zeroth-order term $g(k, s)$ for the gain function at position s along a bunch compressor and wavenumber $k = 2\pi/\lambda$, (λ is the wavelength of the sinusoidal perturbation before compression) has the form [3]

$$g(k,s) = \exp\left(-\frac{1}{2}\,\frac{k^2\sigma_\delta^2 R_{56}^2(s)}{[1+h(s)R_{56}(s)]^2}\right). \tag{57}$$

The beam is assumed to have linear chirp $\alpha(z,s) = \alpha_1(s)z + p_0$. In the notation used in [3] the slope of the chirp is $h(s) = \alpha_1(s)/p_0$. The profile of the R_{56} element of the transfer matrix together with other relevant lattice functions for BC1 are reported in Fig.7.

To determine the gain function numerically, we ran the Vlasov code by adding a small sinusoidal perturbation with amplitude A_i to an initial flattop density and calculated the modulation of the charge density A_f at the end of the bunch compressor. If we denote with ρ_i and ρ_f the peak longitudinal beam densities at the start and end of the bunch compressor, the gain function for the given wavelength is by definition $g = (A_f/\rho_f)/(A_i/\rho_i)$.

The results from the the numerical calculation of the gain function at vanishing current are plotted in Fig. 5 as red dots and compare very well with the analytical expression (57) reported as a solid line.

At finite current, in the presence of CSR alone (space charge not included) the comparison between linear theory and results from numerical solutions are reported in Fig. 6. The good agreement shown was obtained, particularly at small wavelengths, after suitable adjustment of the number of steps Δs in the dipoles. The results shown in the picture were obtained using 20 steps per dipole. Using only 5 steps resulted in a gain at the smallest wavelength evaluated (4 μm) about a factor 2 larger. The integral equation for the gain function from linear theory [2] was solved using a uniform 400-point grid in s.

In Fig. 8 we show an example of beam phase space at the entrance of the 36 m L1-section of the linac preceding the bunch compressor BC1 and at the exit of BC1. The beam has a flat-top charge density with a small sinusoidal perturbation. Only the central portion of the beam density is plotted. In the calculation we included CSR in BC1 and space charge in L1. The latter was responsible for most of the large gain observed at the 20 μm wavelength. The initial beam energy was about 96 MeV.

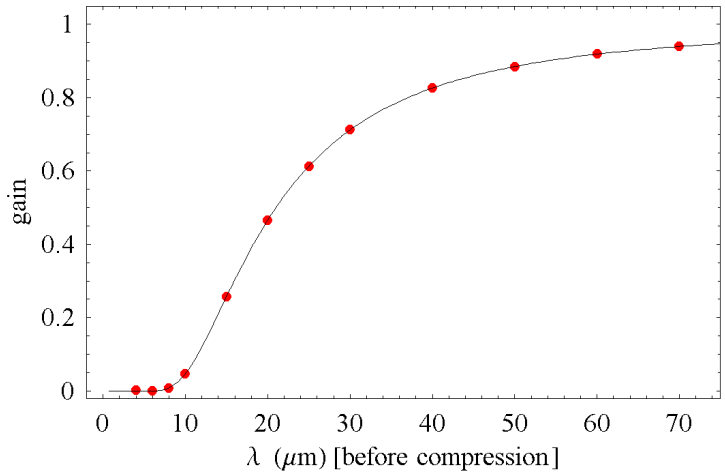

Figure 5: Gain function through the fermi@elettra bunch compressor BC1 at vanishing current, as determined from numerical solutions of the Vlasov equation (dots) and linear theory (solid line), Eq. (57).

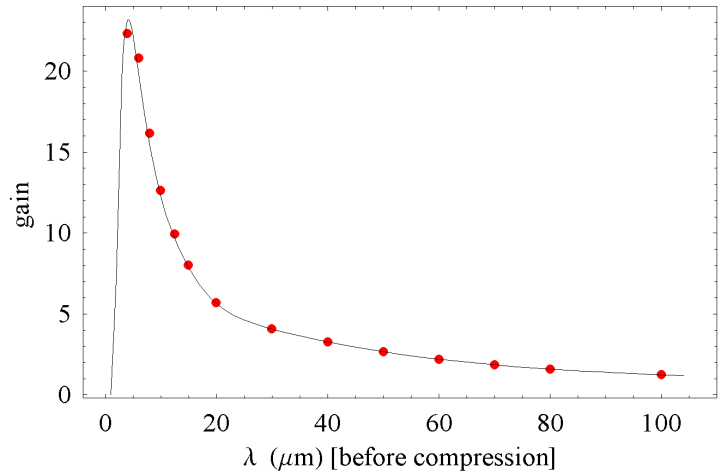

Figure 6: Gain function through the fermi@elettra bunch compressor BC1 at finite current, as determined from numerical solutions of the Vlasov equation (dots) and linear theory (solid line). Peak current $I_0 = 95.5$ A (before compression), $I_0 = 336.2$ A (after compression). CSR is the only collective effect included in the calculation.

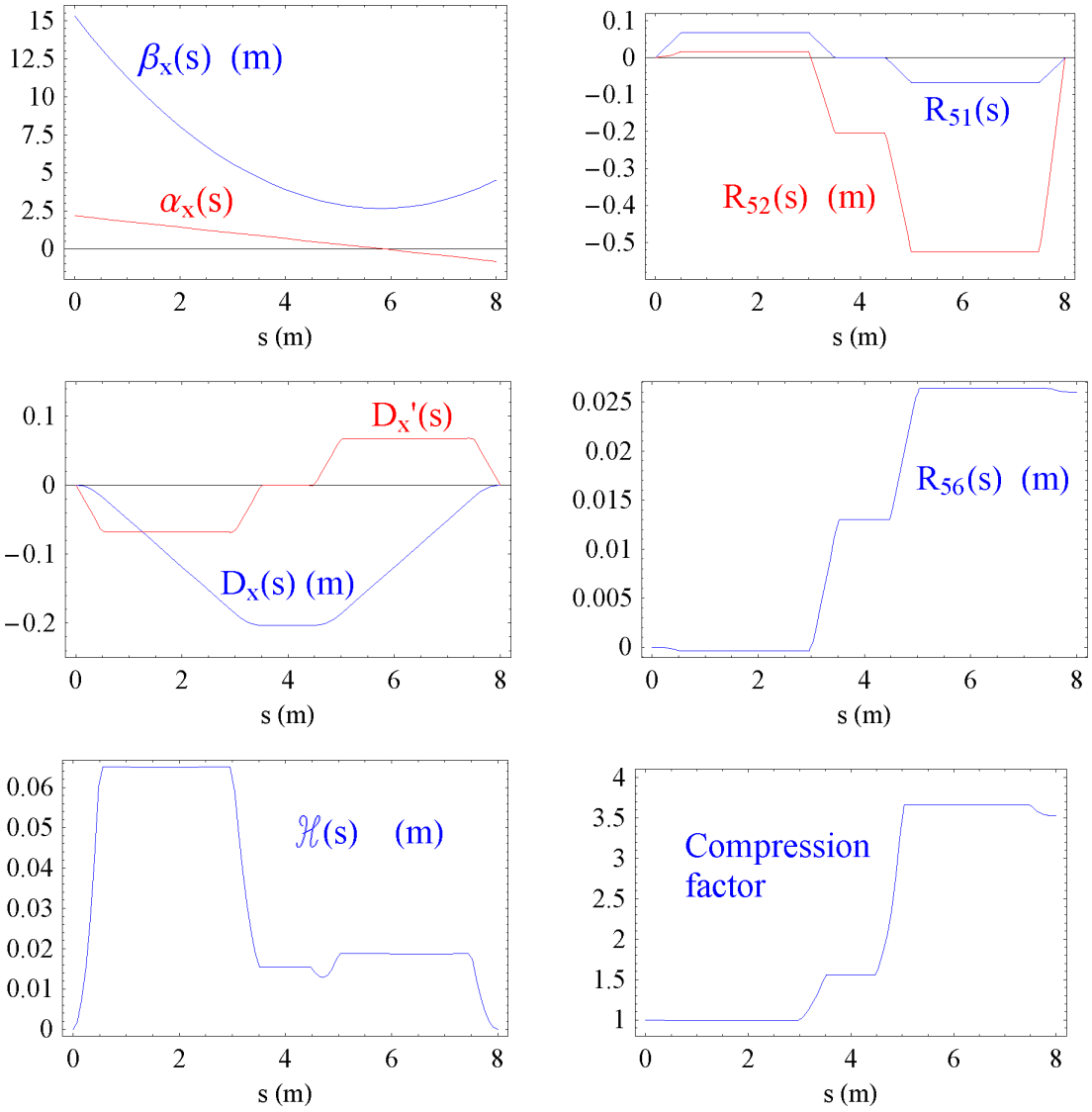

Figure 7: Lattice functions (including the $\mathcal{H}(s)$ function), selected entries of the 'R-matrix', and compression factor for BC1, the first bunch compressor in the fermi@elettra linac.

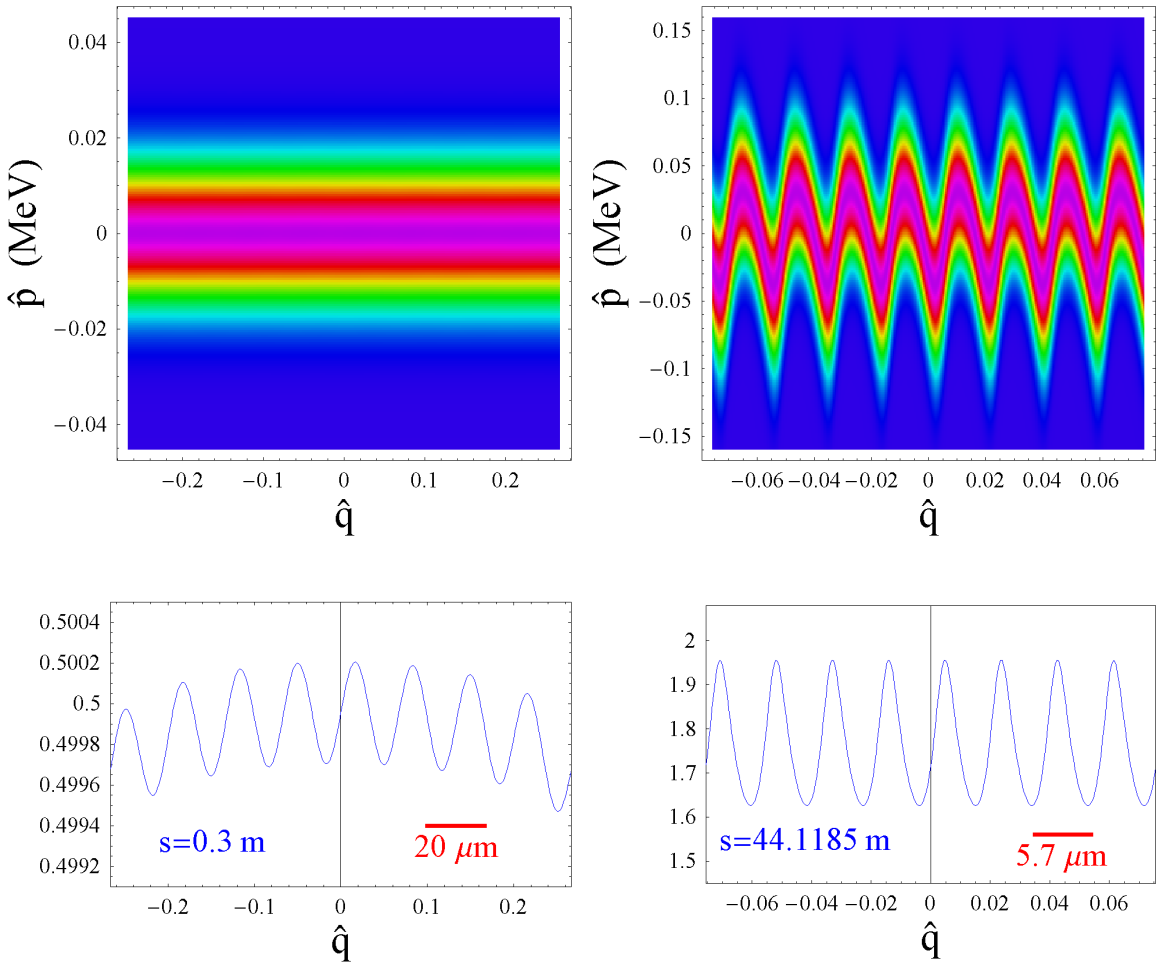

Figure 8: Phase space at start of linac and end of BC1 (top left and right pictures) and corresponding longitudinal densities (bottom pictures) in the presence of space charge and CSR. The initial density function is gaussian in energy and is a smooth flattop in z with half-length $l_b = 0.3$ mm and a superposed 20 μm wavelength sinusoidal modulation. Only the central portion of the beam density is plotted. The gain factor is about 182; $\hat{q} = \hat{z}/l_b$ is the normalized longitudinal coordinate.

7 Approximate Account of Transverse Motion Effects on Longitudinal Dynamics

The most important limitation to a purely 2D model of dynamics is neglect of a smearing effect on microbunching caused in a bunch compressor by a finite horizontal emittance, which may result in substantially smaller gain curves for the microbunching instability [2, 3]. While a fully accurate account requires solving the equations of motion in 4D, we can devise an approximate model under the assumption that the transverse dynamics is little affected by the dynamics in z.

We suppose that we make a (hopefully) small error if we assume that solutions of the 4D Vlasov equation expressed in terms of the 'beta' coordinates, maintains the factorization

$$f = g(x_\beta, p_{x\beta}) f_{z\beta}(z_\beta, \delta_\beta) \tag{58}$$

between longitudinal and transverse motion. For the horizontal distribution we assume a gaussian density matched to the lattice

$$g(x_\beta, p_{x\beta}) = \frac{1}{2\pi\varepsilon_x} \exp\left(-\frac{I_\beta(x_\beta, p_{x\beta})}{2\varepsilon_x}\right), \tag{59}$$

where $I_\beta(x_\beta, p_{x\beta}) = \gamma_x x_\beta^2 + 2\alpha_x x_\beta p_{x\beta} + \beta_x p_{x\beta}^2$ is the familiar Courant invariant. Notice that the factorization (58) would be exactly preserved in the absence of collective effects.

Next, insert the ansatz (58) into the 4D Vlasov equation (17) and find

$$g\frac{\partial f_{z\beta}}{\partial s} - \delta_\beta \frac{D}{R} g \frac{\partial f_{z\beta}}{\partial z_\beta} + F(\zeta) g \frac{\partial f_{z\beta}}{\partial \delta_\beta} + T_\beta = 0, \tag{60}$$

where as in Sec.2, ζ is a shorthand for $\zeta = z_\beta - x_\beta D' + p_{x\beta} D$ and

$$\begin{aligned} F(\zeta) &= e^2 N \int_{-\infty}^{\infty} dz' w(\zeta - z') \int dx dp_x d\delta \; f(x, p_x, z', \delta) \\ &= e^2 N \int_{-\infty}^{\infty} dz' w(\zeta - z') \int dx dp_x d\delta \; g(x - \delta D, p_x - \delta D') f_{z\beta}(z' + xD' - p_x D, \delta) \end{aligned} \tag{61}$$

with

$$T_\beta = -F(\zeta) D \frac{\partial g}{\partial x_\beta} f_{z\beta} - F(\zeta) D' \frac{\partial g}{\partial p_{x\beta}} f_{z\beta}. \tag{62}$$

In writing (60) we exploited the invariance of I_β under the unperturbed dynamics: $dI_\beta/ds = 0$. Finally, we remove the dependence of (60) on the transverse coordinates by averaging and obtain

$$\frac{\partial f_{z\beta}}{\partial s} - \delta_\beta \frac{D}{R} \frac{\partial f_{z\beta}}{\partial z_\beta} + \frac{\partial f_{z\beta}}{\partial \delta_\beta} \int dx_\beta dp_{x\beta} \; F(z_\beta - x_\beta D' + p_{x\beta} D) g(x_\beta, p_{x\beta}) = 0. \tag{63}$$

In writing (63) we exploited the fact that the average of T_β over the transverse phase space vanishes, as it can be seen after integration by parts:

$$\begin{aligned}\int dx_\beta dp_{x\beta} T_\beta &= -f_{z\beta}\int dx_\beta dp_{x\beta}\left(F(\zeta)D\frac{\partial g}{\partial x_\beta}+F(\zeta)D'\frac{\partial g}{\partial p_{x\beta}}\right)\\ &= -f_{z\beta}\int dx_\beta dp_{x\beta}F'(\zeta)(-DD'+DD')g=0. \end{aligned} \tag{64}$$

In Eq. (63) the term

$$F_{\rm sm}(z_\beta)=\int dx_\beta dp_{x\beta}\ F(z_\beta-x_\beta D'+p_{x\beta}D)g(x_\beta,p_{x\beta}) \tag{65}$$

is an effective longitudinal collective force accounting for the smearing from the horizontal emittance.

Upon carrying out some judicious changes of integration variables one can verify that (65) reduces to

$$F_{\rm sm}(z)=e^2N\int_{-\infty}^{\infty}dz'w(z-z')\rho_{\rm sm}(z'), \tag{66}$$

where the smeared longitudinal density $\rho_{\rm sm}(z)$ is given by

$$\rho_{\rm sm}(z)=\int_{-\infty}^{\infty}dt\ \frac{\exp(-t^2/2\sigma_\perp^2)}{\sqrt{2\pi}\sigma_\perp}\rho(z+t), \tag{67}$$

with the amplitude of the smearing $\sigma_\perp=\sqrt{2\varepsilon_x\mathcal{H}}$ depending on the transverse lattice through the 'curly H' function $\mathcal{H}=\gamma_xD^2+2\alpha_xDD'+\beta_x(D')^2$. In frequency domain the smearing has the form of a low-pass filter

$$F_{\rm sm}(z)=-e^2Nc\int_{-\infty}^{\infty}dk\ \hat{Z}(k)\tilde{\rho}(k)e^{ikz}e^{-k^2\sigma_\perp^2/2}, \tag{68}$$

with a cut-off wavelength λ_c defined by $k^2\sigma_\perp^2/2\simeq 1$ yielding $\lambda_c=2\pi\sqrt{\varepsilon_x\mathcal{H}}$.

That the smearing induced by a finite transverse emittance is related to the $\mathcal{H}(s)$ function is not surprising but it appears to have escaped notice. For example, in [3] ** the expression for the gain function in the absence of collective effects is reported as

$$g(k,s)=\exp\left(-\frac{1}{2}\ k^2\sigma_\delta^2R_{56}^2(s)C(s)\right)\exp\left(-\frac{k^2C(s)\varepsilon_x}{2\beta_{x0}}[(\beta_{x0}R_{51}(s)-\alpha_{x0}R_{52}(s))^2+R_{52}^2(s)]\right), \tag{69}$$

where β_{x0} and α_{x0} are the Twiss functions at s_0, $C(s)=1/[1+h(s)R_{56}(s)]$ is the compression factor and $R_{ij}(s)$ are the entries of the transfer matrix for single-particle motion in a bunch compressor from s_0 to s:

$$R_{s_0\to s}=\begin{pmatrix} R_{11}(s) & R_{12}(s) & 0 & D\\ R_{21}(s) & R_{22}(s) & 0 & D'\\ R_{51}(s) & R_{52}(s) & 1 & R_{56}(s)\\ 0 & 0 & 0 & 1\end{pmatrix}. \tag{70}$$

**A similar expression also appears in [2] but is less general in that it is assumed that the lattice function $\alpha_x(0)=0$.

Having assumed that at $s = s_0$, $R_{11}(s_0) = R_{22}(s_0) = 1$, whereas all other off-diagonal entries vanish, we have $R_{51}(s) = R_{21}(s)D(s) - R_{11}(s)D'(s)$ and $R_{52}(s) = R_{22}(s)D(s) - R_{12}(s)D'(s)$.

It can be verified that in equation (69) the expression in the [ ] brackets reduces to

$$[(\beta_{x0}R_{51}(s) - \alpha_{x0}R_{52}(s))^2 + R_{52}^2(s)]/\beta_{x0} = \mathcal{H}(s). \tag{71}$$

Verification of (71) can be done by direct substitution, using the rule for propagating the lattice functions [20]

$$\begin{pmatrix} \beta_x(s) \\ \alpha_x(s) \\ \gamma_x(s) \end{pmatrix} = \begin{pmatrix} R_{11}^2 & -2R_{11}R_{12} & R_{12}^2 \\ -R_{11}R_{21} & (R_{11}R_{22} + R_{12}R_{21}) & -R_{12}R_{22} \\ R_{21}^2 & -2R_{21}R_{22} & R_{22}^2 \end{pmatrix} \begin{pmatrix} \beta_{x0} \\ \alpha_{x0} \\ \gamma_{x0} \end{pmatrix}, \tag{72}$$

where $R_{ij} = R_{ij}(s)$.

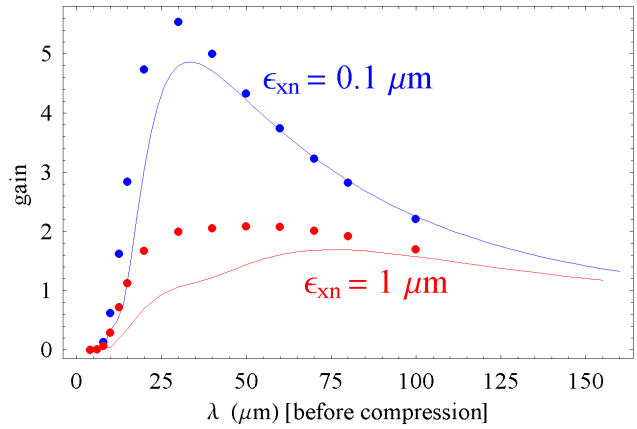

Figure 9: Comparison between model of smearing from horizontal emittance discussed in this section (dots) and linear theory (lines). The gain curves are for the fermi@elettra first bunch compressor (BC1) and are shown for two values of normalized horizontal emittance. The beam peak current (before compression) is $I = 191.1$ A in both cases. The beam energy is E=233 MeV, the energy spread $\sigma_p = 10$ KeV.

As a way to gain some confidence in our calculation we compared the gain function for finite emittance as obtained from the model described in this section and linear theory [2]. For this purpose we carried out two sets of calculations. In the first set we evaluated the gain function though the bunch compressor BC1 in the presence of CSR only (*i.e.* space charge was not included) for a beam current $I = 191$ A (before compression): this value, which is twice the fermi@elettra design specification, was set to enhance the effect of CSR. We considered two values of horizontal emittance. The results are reported in Fig. 9 as dots. The solid lines are from linear theory. We observe some discrepancy at larger emittance. The agreement, however, becomes better at smaller emittance.

In the second set of calculations we included the L1 section of the fermi@elettra linac preceding BC1 and turned on space-charge in L1 (but CSR was the only collective effect

present in the bunch compressor). At the entrance of the L1 section the beam is at an energy of about $E = 96$ MeV and is accelerated to $E = 233$ MeV as it enters BC1 after travelling through five RF structures (including one linearizer yielding no net acceleration). The length of L1 is about 36 m. Space charge kicks as determined using the impedance (24) were applied once at the end of each drift and quadrupole, and 10 times within each cavity. The additional number of kicks applied in the cavities is required by the strong dependence of space charge on beam energy.

In the calculation we defined the r_b parameter (see (24)) as $r_b = 1.3\sqrt{(\sigma_x^2 + \sigma_y^2)/2}$, where $\sigma_x^2 = \beta_x \varepsilon_x$, $\sigma_y^2 = \beta_y \varepsilon_y$ are the local values of the transverse rms beam sizes (where we assumed $\gamma\varepsilon_x = \gamma\varepsilon_y = 1$ μm). The factor 1.3 is an attempt to adjust the space-charge model to account for the actual transverse density distribution of the physical beam, which is closer to gaussian than uniform (recall that the impedance (24) presupposes a beam with uniformly transverse density and circular cross-section).

The calculation was done for a peak current $I = 95.5$ A (before compression). The gain functions through L1+BC1 are shown in the two pictures in Fig.10 as red dots and contrasted with the gain curves from linear theory (solid lines) for two values of the normalized horizonal emittance.

In the model of space charge used in the linear theory calculation, the beam radius r_b was assumed to be uniform in z and set to $r_b = 0.28$ mm, a value obtained by taking the s-average of $1.3\sqrt{[\sigma_x^2(s) + \sigma_y^2(s)]/2}$ over the length of the linac L1.

By comparing the two pictures in Fig.10 we can appreciate the considerable impact that a $\varepsilon_{xn} = 1$ μm horizontal emittance has on softening the gain function. The agreement with linear theory is satisfactory but, we should emphasize, this is for a case where the overwhelming contribution to the gain function results from space charge in the linac trailing the bunch compressor.

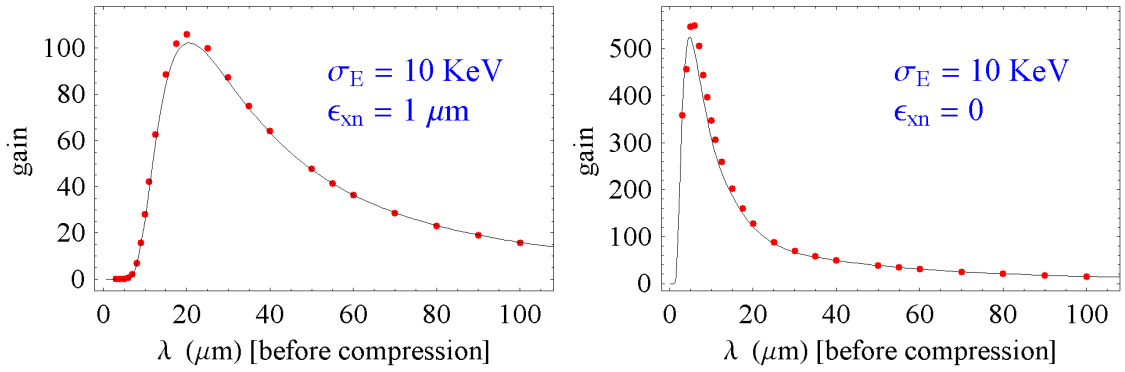

Figure 10: Gain curves through L1 and BC1 as determined from linear theory (solid line) and numerical solutions of the Vlasov equation, with non-vanishing (left picture) and vanishing (right-picture) transverse emittance. Space charge was included in L1 but not in BC1 and calculated based on the beam sizes resulting from $\gamma\varepsilon_x = \gamma\varepsilon_y = 1$ μm in both pictures. CSR was included in BC1.

8 Discussion and Conclusions

A pleasant feature of the 2D Vlasov solver we have presented is a model promising to account for an effective description of the smearing effect of a finite horizontal emittance on microbunching without the need to follow the horizontal dynamics. However, the accuracy of the model, which we have introduced on a purely heuristic basis, remains to be assessed. The partial agreement we found between our model and results from linear theory is interesting, but calls for further clarification. The treatment of transverse effects in the linear model is exact except for the effect of linearization, whereas our averaging on betatron coordinates without linearization results in a different approximation.

We should conclude by pointing to some of the known limitations of our Vlasov solver, at least in its present form. While it appears to be fully adequate for the study of microbunching, as it affects a beam on a short length scale, features of the beam density on a longer scale (including large energy spread developing at the ends of flat-top beams or curvatures of the beam densities due to the RF wave nonlinearities and RF structure wake fields) may not be properly handled at this time. We have yet to carry out a systematic investigation of this point but two difficulties can be anticipated, which would require some substantial refinement of the technique discussed in this paper.

The first difficulty would arise if collective forces substantially affected the beam position/energy correlation in the longitudinal phase space. This would make it necessary to redefine the rule for the evolution of the chirp function α so as to include the effect of the collective force and maintain the support of the beam density centered in the grid used to represent the beam density. Implementing this poses no problem in principle. However, depending on the specifics of a given linac design and beam parameters it could happen that the correlation function α may become multi-valued, making the coordinate transformation (30), (31) ill defined. An obvious solution to this difficulty would be to distinguish between the regions of phase space where the transformation can be uniquely defined and apply the method of Sec. 3 to each region separately. It remains to be seen whether this prescription would be practical and efficient.

A second difficulty could be caused by a substantial spreading of the support of the beam density in phase space. If this spreading was localized (typically at the head and tail of the beam), a rectangular grid to represent the beam density could become very inefficient. A hint to this problem is already apparent in the bottom-right picture of Fig. 3 where the center of the beam support is shown to be shifting downward while the particles at the beam ends show relative energy gain. A grid adaptation scheme more sophisticated than the one discussed in this paper could be necessary. Perhaps, a locally cartesian grid with adapting boundary might offer a manageable solution.

9 Acknowledgments

Discussions with and comments from G. Bassi, J. Ellison, P. Emma, B. Fawley, and Z. Huang are gratefully acknowledged.

References

[1] E.L. Saldin, E.A. Schneidmiller, and M.V. Yurkov, Nucl. Instrum. Methods Phys Res., Sect. A **483**, 516 (2002).

[2] S. Heifets, G. Stupakov, and S. Krinsky, Phys. Rev. ST Accel. Beams **5**, 064401 (2002).

[3] Z. Huang and K-J. Kim, Phys. Rev. ST Accel. Beams **5**, 074401 (2002).

[4] Z. Huang, M. Borland, P. Emma, J. Wu, C. Limborg, G. Stupakov, and J. Welch, Phys. Rev. ST Accel. Beams **7**, 074401 (2004).

[5] C. Z. Cheng and G. Knorr, J. Comput. Phys. **22**, 330 (1976).

[6] O. Boine-Frankenheim, I. Hofmann, and G. Rumolo, Phys. Rev. Lett. **82**, 3256 (1999).

[7] E. Sonnendrücker, J. Roche, P. Bertrand, and A. Ghizzo, J. Comput. Phys. **149**, 201 (1999).

[8] R. Warnock and J. Ellison, in Proceedings of the 2nd ICFA Advanced Workshop on Physics of High Brightness Beams, Los Angeles, 1999 (World Scientific, Singapore, 2000); also available as SLAC-PUB-8404, 2000.

[9] M. Venturini and R. Warnock, Phys. Rev. Lett. **89**, 224802 (2002).

[10] M. Venturini, R. Warnock, R. Ruth, and J. A. Ellison, Phys. Rev. ST Accel. Beams **8**, 014202 (2005).

[11] R. Warnock, Nucl. Instrum. Methods Phys. Res., Sect. A **561**, 186 (2006).

[12] R. Warnock, G. Bassi, and J. Ellison, Nucl. Instrum. Methods Phys. Res., Sect. A **558**, 85 (2006).

[13] A. Sobol, *A Vlasov Treatment of the 2DF Collective Beam-Beam Interaction: Analytical and Numerical Results*, Ph.D. Dissertation, Mathematics, University of New Mexico (July 2006).

[14] M. Gutnic, M. Haefele, and E. Sonnendrücker, Nucl. Instrum. Methods Phys. Res., Sect. A **558** 159 (2006); M. Mehrenberger, E. Violard, O. Hoenen, M. Campos Pinto, and E. Sonnendrücker, *ibid.* 188.

[15] J. Behrens and A. Iske, Computers and Mathematics with Applications **43**, 319 (2002).

[16] C. Bocchetta *et al.*, Proc. of the EPAC06 Conf., Edinburgh, UK (June 2006).

[17] A. Chao, *Physics of Collective Beam Instabilities in High Energy Acceleratos* (John Wiley & Sons, Inc., New York 1993).

[18] R. Ruth, in *Nonlinear Dynamics Aspects of Beam Dynamcis, Lecture Notes in Physics* (Springer-Verlag, Berlin, 1986).

[19] J. Rosenzweig, C. Pellegrini, L. Serafini, C. Ternieden, and G. Travish, Nucl. Instrum. Methods Phys. Res., Sect. A **393**, 376 (1997).

[20] S.Y. Lee, *Accelerator Physics* (World Scientific, Singapore, 1999).

[21] M. Cornacchia *et al.*, Study of the Electron Beam Dynamcis in the Fermi@Elettra Linac, Proc. of the EPAC06 Conf., Edinburgh, UK (June 2006).